Journal of Magnetic Resonance **157,** 31–42 (2002)
doi:10.1006/jmre.2002.2567

Quantitative Measurement of Two-Dimensional Distribution Functions of Diffusion and Relaxation in Grossly Inhomogeneous Fields

M. D. Hürlimann[1] and L. Venkataramanan

Schlumberger-Doll Research, Old Quarry Road, Ridgefield, Connecticut 06877-4108

Received December 4, 2001; revised May 14, 2002

We demonstrate the quantitative extraction of multidimensional distribution functions in the presence of grossly inhomogeneous fields. Examples are shown for diffusion—T_2 distribution functions and $T_1 - T_2$ distribution functions. The pulse sequences consist of an initial editing sequence followed by a long series of nominal 180° pulses. They are designed such that the kernels describing the relationships between the distribution functions and the measured data are separable. The required phase cycling is discussed. We analyze in detail the extra spin dynamics effects due to the strong field inhomogeneities including the effects on diffusion and relaxation. A recently developed algorithm is used to invert the data and extract stable multidimensional distribution functions in an efficient manner. We present examples for several applications of this new technique. Diffusion–relaxation distribution functions can be used for fluid identification and for the characterization of pore geometry of porous media based on the effects of restricted diffusion. We have also determined $T_1 - T_2$ distribution functions of water saturated sedimentary rock and find excellent agreement with previous measurements performed in homogeneous fields.

Key Words: **strayfield NMR; multidimensional distribution function; relaxation; diffusion; CPMG; inhomogeneous fields.**

1. INTRODUCTION

NMR diffusion (*1–3*) and relaxation measurements (*4–6*) have become important tools to study the structure of porous media, ranging from biological systems to hydrocarbon bearing sedimentary rocks. In recent years, "inside–out" instrumentation has been developed to extend NMR measurements to samples that do not fit into the bore of a standard NMR magnet. Applications include well logging, i.e., the evaluation of earth formations from a borehole (*7*); materials testing with one-sided NMR devices for the evaluation of objects such as tires and construction materials (*8*); and sensitive diffusion measurements with strayfield NMR setups (*9, 10*).

When the sample sits outside the measuring device, the applied dc and RF fields across the sample are necessarily strongly inhomogeneous, with inhomogeneities that are typically much larger than the nominal RF field strength. Under such conditions, it is in general not possible to obtain spectroscopic information, unless there are special correlations between the B_0 and B_1 inhomogeneities and special pulse sequences are used (*11*). Every pulse acts as a slice selective pulse and the exact spin dynamics of any multipulse sequence becomes quickly very complex. We have recently analyzed relaxation and diffusion effects for general pulse sequences in such inhomogeneous fields (*12, 13*) and shown that it is possible to extract quantitatively diffusion coefficients and relaxation times.

Here we demonstrate that it is possible to measure multidimensional distribution functions involving diffusion, longitudinal, or transverse relaxation, even in the presence of strong inhomogeneities of the applied fields. Such multidimensional distribution functions contain inherently more information than one-dimensional distribution functions and are useful for a range of different applications that we present.

In this paper, we first discuss the pulse sequences underlying this technique. We analyze the spin dynamics including diffusion and relaxation effects, under full treatment of the off-resonance effects. The case for diffusion—T_2 correlation measurements is treated in detail in the Appendix, including the required phase cycling. The main theoretical predictions are then verified experimentally. We demonstrate the successful extraction of both $D - T_2$ and $T_1 - T_2$ distribution functions for applications of fluid typing and for the characterization of the geometry of porous media.

2. PULSE SEQUENCES FOR $D - T_2$ AND $T_1 - T_2$ DISTRIBUTION FUNCTIONS

The measurement of two-dimensional distribution functions between two dissipative quantities x_1 and x_2 (such as relaxation and diffusion) is based on sequences where two or more independent times are varied in such a way that the kernel separates out. The measured magnetization $M(t_1, t_2)$ then depends on the quantities of interest x_1 and x_2 through

$$M(t_1, t_2) = \iint dx_1\, dx_2\, f(x_1, x_2)\, k_1(x_1, t_1)\, k_2(x_2, t_2). \quad [1]$$

[1] To whom correspondence should be addressed. E-mail: hurlimann@ridgefield.sdr.slb.com.

1090-7807/02 $35.00

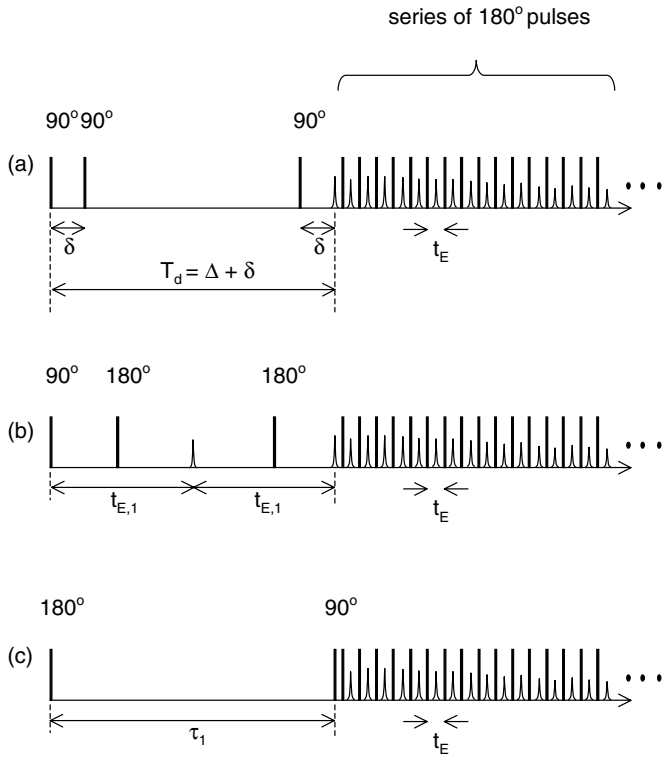

FIG. 1. Pulse sequence to measure 2D distribution functions. The first two sequences are examples of diffusion editing sequences, followed by the CPMG sequence. In the first sequence (a), the diffusion editing is achieved with a stimulated echo, whereas in the second sequence (b), a direct echo with increased echo spacing is used. The bottom sequence (c) is a T_1 editing sequence, followed by CPMG detection. In this example, the T_1 editing is achieved by an inversion–recovery sequence.

Here $f(x_1, x_2)$ is the distribution function of interest and k_1 and k_2 are the kernels. These experiments are analogous to conventional multidimensional NMR spectroscopy, where the kernels are typically phase factors of the form $e^{i\alpha x_1 t_1}$ and the distribution function $f(x_1, x_2)$ is obtained from $M(t_1, t_2)$ by multidimensional Fourier transformation. In contrast, the kernels for relaxation and diffusion measurements are generally of an exponential form, $e^{-\alpha x_1 t_1}$, and the data inversion requires a multidimensional inverse Laplace transformation.

Examples of pulse sequences to measure diffusion–relaxation and relaxation–relaxation cross correlations are shown in Fig. 1. These pulse sequences consists of two distinct parts. The initial part can be thought of as an editing sequence where the signal is made sensitive to one of the quantity of interest, such as T_1 relaxation or diffusion. This is followed by a long series of 180° pulses, used to determine the T_2 relaxation time. All sequences in Fig. 1 are generalized CPMG sequences, where the "editing" sequence replaces the standard 90° pulse of the CPMG sequence.

In the first sequence shown in Fig. 1, the initial editing sequence consists of a stimulated echo sequence. By varying the time δ, the sensitivity to diffusion can be varied systematically. For this reason, we call this a *diffusion editing* sequence. This sequence for static gradients is similar to the sequence used by Peled *et al.* [14] with pulsed gradients. In the second sequence, the diffusion sensitivity is achieved by a direct echo sequence where the initial echo spacings $t_{E,1}$ are varied. The third sequence shown in Fig. 1 can be used to measure $T_1 - T_2$ correlations and consists of an initial 180°–90° inversion recovery sequence followed by the standard CPMG sequence. In all these sequences, it is advantageous to set the echo spacings in the second part of the sequences, t_E, short enough to make the decay times independent of diffusion.

3. MEASUREMENTS IN GROSSLY INHOMOGENEOUS FIELDS

For the sequences shown in Fig. 1, it is straightforward to list the kernels $k_1(x_1, t_1)$ and $k_2(x_2, t_2)$ for the on-resonance case. For spins with relaxation times T_1 and T_2, diffusing in a constant gradient g with a diffusion coefficient D, they are given by

$$k^o_{1,a}(D, \delta) = \frac{1}{2}\exp\left\{-\gamma^2 g^2 \delta^2 D\left(\Delta - \frac{\delta}{3}\right)\right\} \times \exp\left\{-\frac{\Delta + \delta}{T_1} - 2\delta\left(\frac{1}{T_2} - \frac{1}{T_1}\right)\right\} \quad [2]$$

$$k^o_{1,b}(D, t_{E,1}) = \exp\left\{-\frac{1}{6}\gamma^2 g^2 D t^3_{E,1}\right\}\exp\left\{-\frac{2t_{E,1}}{T_2}\right\} \quad [3]$$

$$k^o_{1,c}(T_1, \tau_1) = 1 - 2\exp\left\{-\frac{\tau_1}{T_1}\right\} \quad [4]$$

$$k^o_2(T_2, kt_E) = \exp\left\{-\frac{kt_E}{T_2}\right\}. \quad [5]$$

In these expressions, the superscript o indicates that they apply on-resonance and the second subscript in k_1 specifies the sequence. In strongly inhomogeneous fields, the situation is complicated because all pulses become slice selective and the kernels depend in general on the offset frequency. This complication can be overcome with proper phase cycling, so that the kernels for inhomogeneous fields retain approximately the general form of Eqs. [2]–[5].

To calculate the kernels relevant for grossly inhomogeneous fields, the analysis of the spin dynamics of the many-pulse sequences shown in Fig. 1 has to include the effects of diffusion, relaxation, and strong field inhomogeneities. It is natural to divide the analysis of the sequence into its two distinct parts, the initial "editing" sequence followed by the repeated refocusing. A detailed discussion of the spin dynamics for the two parts can be found in Appendix A for the sequence of Fig. 1a. Here we give a brief summary.

The "editing" part of the sequence consists of only a few pulses and the spin dynamics can be determined exactly by

TABLE 1
Phase Cycling for the Diffusion Editing Sequence with Stimulated Echo

ϕ_1	ϕ_2	ϕ_3	ϕ_{180}	ϕ_{acq}
0	0	0	$\pi/2$	π
π	0	0	$\pi/2$	0
0	π	0	$\pi/2$	0
π	π	0	$\pi/2$	π
0	0	π	$\pi/2$	0
π	0	π	$\pi/2$	π
0	π	π	$\pi/2$	π
π	π	π	$\pi/2$	0
$\pi/2$	0	0	0	$\pi/2$
$-\pi/2$	0	0	0	$-\pi/2$
$\pi/2$	π	0	0	$-\pi/2$
$-\pi/2$	π	0	0	$\pi/2$
$\pi/2$	0	π	0	$-\pi/2$
$-\pi/2$	0	π	0	$\pi/2$
$\pi/2$	π	π	0	$\pi/2$
$-\pi/2$	π	π	0	$-\pi/2$

Note. The phases of the first three 90° pulses, ϕ_1, ϕ_2, and ϕ_3, the phase of all the 180° pulses, ϕ_{180}, and the acquisition phase, ϕ_{acq}, are cycled through these 16 steps to select the stimulated echo contributions.

considering all possible coherence pathways (*13*). This allows us to calculate the spectrum and dependence on diffusion and relaxation of the magnetization at the end of the editing sequence, $\vec{m}_{\mathcal{A}}$. A key point is that we use a phase cycling (given in Table 1) such that a single coherence pathway is selected. This results in the simple diffusion dependence $\exp\{-\gamma^2 g^2 \delta^2 D(\Delta - \frac{\delta}{3})\}$ that is uniform across the whole spectrum.

In the second part of the sequence, the magnetization $\vec{m}_{\mathcal{A}}$ is repeatedly refocused by a long series of 180° pulses to obtain the relaxation information. The exact spin dynamics of a long series of refocusing pulses in strongly inhomogeneous fields becomes very complicated, because each pulse creates new coherence pathways. The situation can be greatly simplified by reducing the echo spacing t_E sufficiently to make the diffusion effect insignificant in this part of the sequence. This allows us to use the "effective rotation axis" approach (*12, 15*). After a short transient that extends over only a few echoes, the echoes approach an asymptotic shape with a simple relaxation decay. Using the notation of Appendix A, the magnetization after the first few echoes can be written as

$$\vec{m}(kt_E) \approx \hat{n}(\hat{n} \cdot \vec{m}_{\mathcal{A}}) \exp\{-t/T_{2\text{eff}}\}. \qquad [6]$$

Here $\hat{n}$ is the effective rotation axis describing the refocusing cycle (given in Eqs. [18] and [19]), $\vec{m}_{\mathcal{A}}$ is the magnetization at the end of the editing sequence (given in Eq. [13]), and the effective relaxation rate $1/T_{2\text{eff}}$ is a weighted average of $1/T_2$ and $1/T_1$ (given in Eq. [23]). Note that in this implementation, the dependence of the magnetization on diffusion and relaxation remains separable and exponential.

3.1. Experimental

We performed measurements in the fringefield outside a horizontal bore 2-T superconducting magnet. The NMR probe and sample were placed 0.5 m outside the end of the magnet, where the ^{1}H Larmor frequency is 1.764 MHz with a constant static gradient of 13.2 G/cm.

The samples are typically 2 cm in diameter and 3.75 cm in length. In our geometry, RF pulses excite a slice along the axis of the sample. With pulse durations of $t_{180} = 24\ \mu$s, the slice thickness is about 7.8 mm. Note that the sample diameter significantly exceeds this slice thickness. We describe here experiments with samples that include water, hydrocarbon oil, and rock cores saturated with brine. In some cases we used $NiCl_2$ to reduce the relaxation times of water to $T_1 = T_2$ to 202 ms. The hydrocarbon sample was a petroleum based viscosity standard, called S3,[2] with a kinematic viscosity of 4 mm^2/s at 25°C.

3.2. Testing of Phase Cycling

We have tested the key features of the spin dynamics calculations in Appendix A that leads to Eq. [6] with measurements on a sample of water. In Fig. 2, the stimulated echo followed by the first ten echoes are shown for five different values of δ and a fixed diffusion encoding time of $T_d = 20$ ms. The values of δ were chosen such that for the diffusion coefficient of water, D, the exponent of the diffusion term, $\gamma^2 g^2 \delta^2 D(\Delta - \frac{\delta}{3}) = 0.2, 0.4, 0.6, 0.8, 1$.

The results in Fig. 2 validate the phase cycling. Increasing δ leads to an overall signal decrease by diffusional attenuation without changing the shapes of any of the echoes. This confirms that the diffusion attenuation is uniform for all offset frequencies because a single coherence pathway has been selected.

3.3. Echo Shape

Within a given trace of Fig. 2 there is a significant variation in echo shape between the stimulated echo and the first three echoes. Afterwards, the echo shapes change very little and approach an asymptotic shape. For these later echoes, the second and third terms in Eq. [17] have averaged out and the shape is determined solely by the first term, which is independent of echo number. This asymptotic spectrum, $S(\Delta\omega_0)$, is given by

$$S(\Delta\omega_0) = \int d\omega_1 F(\Delta\omega_0, \omega_1) \times \mathcal{R}e\left\{\Lambda^{(3)}_{+1,0}\Lambda^{(2)}_{0,-1}\Lambda^{(1)}_{-1,0} e^{+i2\Delta\omega_0 t_{90}/\pi}\right\} n_y^2. \qquad [7]$$

Here $F(\Delta\omega_0, \omega_1)$ is the joint distribution function of the offset of Larmor frequency, $\Delta\omega_0$, and of the RF field strength, ω_1, over the sample. We have assumed that the initial pulse spacing δ has been reduced by $2t_{90}/\pi$ to compensate for finite pulse duration effects which gives rise to the extra phase factor (13).

[2] Cannon Instrument Company, P.O. Box 16, State College, PA 16804-0016.

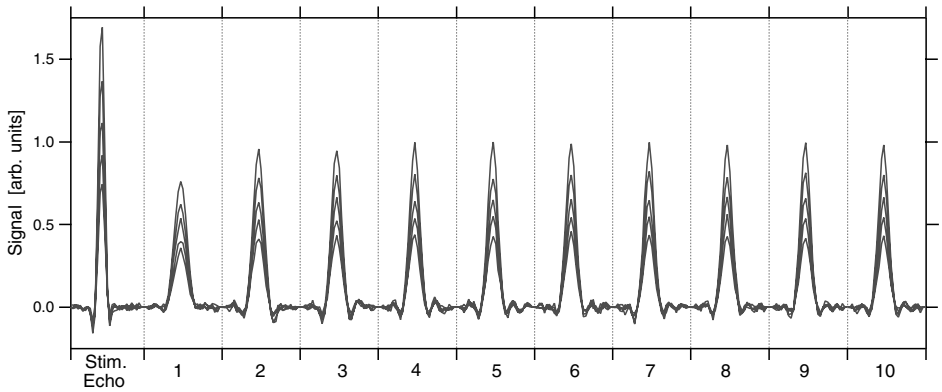

FIG. 2. Measured signals of the stimulated echo and the following first 10 echoes for the diffusion editing sequence shown in Fig. 1a. The 5 traces correspond to different values of δ, each with $T_d = 20$ ms. The sample is water and the measurement was preformed at a frequency of 1.764 MHz in the strayfield outside a 2-T superconduction magnet. The acquisition time for each echo is 160 μs; the echo spacing is 375.2 μs.

A comparison of experimental and theoretical echo shapes is shown in Fig. 3. The theoretical curve was obtained by Fourier transformation of Eq. [7], assuming a B_0 field with a constant gradient and a uniform B_1 field, appropriate for our experimental condition. The agreement is excellent.

3.4. Transient Effect in Initial Echo Amplitudes

As a first step in the data analysis, we extract echo amplitudes from the measured NMR signal. Optimal signal-to-noise ratio is obtained by using the expected echo shape as matched filter. For simplicity, we use the asymptotic echo shape shown in Fig. 3 as a filter for all echoes. In Fig. 4, we show the first 20 amplitudes extracted from the data shown in Fig. 2 for the shortest value of δ. In this case, the relaxation time is much longer than the echo spacing and the echo amplitudes are almost constant after a pronounced transient of the first 2 echo amplitudes. The initial amplitude corresponds to the stimulated echo. Its amplitude and the amplitudes of the first few CPMG echoes have contributions from the second and third terms in Eq. [17] leading to the transient similar to the effect observed with the standard CPMG sequence in inhomogeneous fields (*12*).

This transient depends only on the B_0 and B_1 field distributions and the filter used and it is independent of diffusion or other properties of the sample. We can therefore determine this transient initially either experimentally or theoretically by using Eq. [17] for the magnetization and Eq. [7] for the filter. Figure 4 shows excellent agreement between these two approaches. Using this calibration, we correct the first few echo amplitudes of all our data for this transient effect.

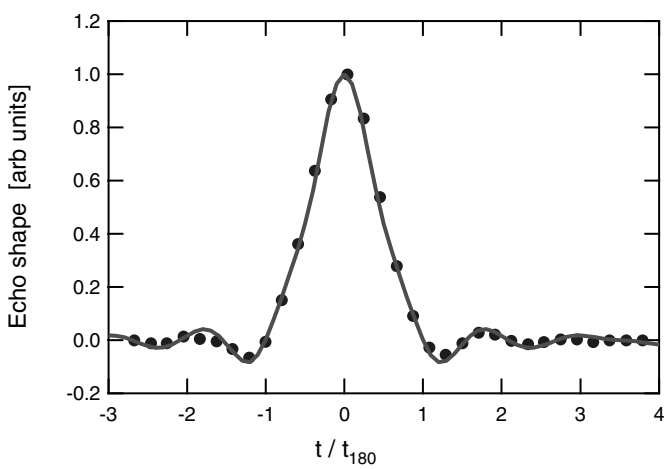

FIG. 3. Comparison of measured (dots) and calculated (solid line) asymptotic echo shape for the stimulated echo–CPMG sequence. Both echoes have been normalized with respect to their peak value. There are no other adjustable parameters.

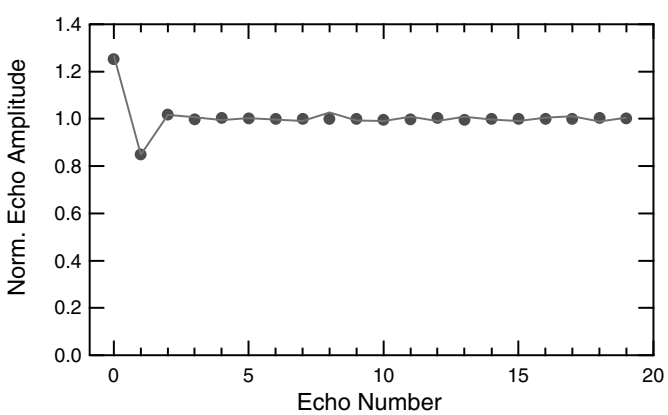

FIG. 4. Transient effect due to spin dynamics in grossly inhomogeneous fields: Experimental results (dots) are compared with theoretical results (line) of echo amplitudes for the stimulated echo and subsequent 19 echoes obtained with matched filtering, using the asymptotic echo shape of Fig. 3. The relaxation time of the water sample is much longer than the echo spacing of 375.2 μs. The transient effect is independent of diffusion.

3.5. Kernels for Inhomogeneous Fields

The extracted echo amplitudes, corrected for the initial transient effect, are then described by

$$A(t,\delta) = \iiint dD\, dT_{2\text{eff}}\, dT_1\, f(D, T_{2\text{eff}}, T_1) \exp\left\{-\frac{T_d}{T_1}\right\} \times \exp\left\{-2\delta\left(\frac{1}{T_2} - \frac{1}{T_1}\right)\right\} \exp\left\{-q^2 D\left(\Delta - \frac{\delta}{3}\right)\right\} \times \exp\left\{-\frac{t}{T_{2\text{eff}}}\right\}. \quad [8]$$

Data are acquired with a fixed total encoding time, $T_d = \Delta + \delta$, for several values of δ. In practice, $\delta \ll T_d$, so that the term $\exp\{-2\delta(\frac{1}{T_2} - \frac{1}{T_1})\}$ can be neglected compared to $\exp\{-T_d/T_1\}$. It is useful to introduce the two-dimensional distribution function $f_{T_d}(D, T_{2\text{eff}})$:

$$f_{T_d}(D, T_{2\text{eff}}) \equiv \int dT_1\, f(D, T_{2\text{eff}}, T_1) \exp\left\{-\frac{T_d}{T_1}\right\}. \quad [9]$$

This is the diffusion–relaxation time distribution function for spins surviving at time T_d. We can then rewrite Eq. [8] as

$$A(t,\delta) = \iint dD\, dT_{2\text{eff}}\, f_{T_d}(D, T_{2\text{eff}}) \times \exp\left\{-q^2 D\left(\Delta - \frac{\delta}{3}\right)\right\} \exp\left\{-\frac{t}{T_{2\text{eff}}}\right\}. \quad [10]$$

This expression for the processed echo amplitudes corresponds closely to the kernels listed in Eqs. [2] and [5] for the on-resonance condition. The only difference is that the transverse relaxation time T_2 is replaced by the effective relaxation time $T_{2\text{eff}}$. Otherwise, the effects of strong inhomogeneities are only reflected in the echo shape and the transient effect. Equation [10] shows that the two-dimensional distribution function $f_{T_d}(D, T_{2\text{eff}})$ is related to the measured echo amplitudes by a two-dimensional inverse Laplace transformation. To extract the correlation quantitatively we used an inversion scheme that is based on an algorithm initially developed to analyze $T_1 - T_2$ measurements (*16*). Details of the algorithm can be found in (*17*). A summary and issues specific to the current application are presented in Appendix B.

3.6. Experimental Data

3.6.1. Doped Water

We performed measurements on $NiCl_2$ doped water to test the method of amplitude extraction and accuracy of Eq. [10]. In Fig. 5, extracted echo amplitudes, transient corrected, are shown for 24 different values of δ with a total encoding time $T_d = 30$ ms. All 24 traces show an exponential decay with identical decay times $T_{2\text{eff}} = 202$ ms that coincide with the independently measured relaxation times $T_2 = T_1$. The relative amplitudes of the 24 traces are plotted versus $\gamma^2 g^2 \delta^2 D(\Delta - \delta/3)$ in the insert. The data are in excellent agreement with the expected decay for the diffusion coefficient of water, $D = 2.3 \times 10^{-9}$ m^2/s, shown as the solid line, over more than two decades. The water data in Fig. 5 are therefore fully consistent with Eq. [10] using a delta function as distribution function $f_{T_d}(D, T_{2\text{eff}})$, centered around the diffusion coefficient of water and relaxation time of the doped $NiCl_2$ solution. This demonstrates that even in the presence of strong field inhomogeneities in excess of B_1, it is possible to make quantitative measurements of diffusion–relaxation time distribution functions.

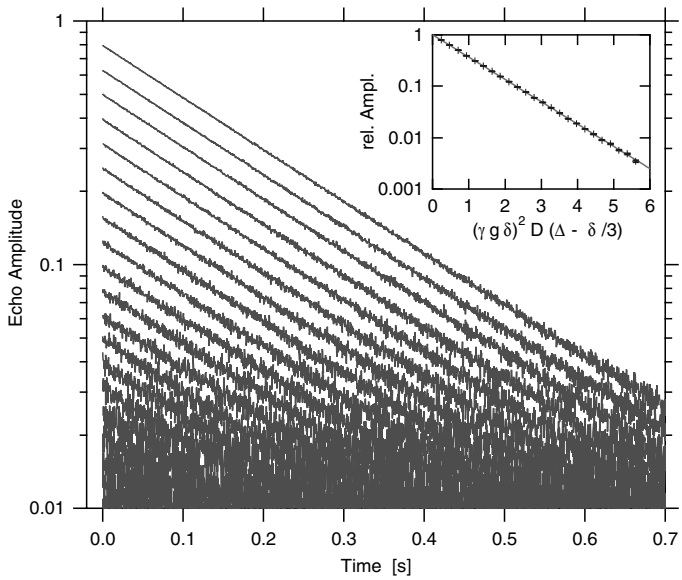

FIG. 5. Results of fringefield measurements with diffusion editing sequence on doped water. Echo amplitudes are plotted versus time after the stimulated echo for 24 different values of diffusion editing, δ. The encoding time T_d was 30 ms. The echo amplitudes were extracted from the data using the asymptotic echo shape in Fig. 3 and the first few amplitudes were corrected for the transient effect as shown in Fig. 4. All traces exhibit identical exponential decays with the expected decay time $T_2 = T_1 = 202$ ms. The insert shows the relative amplitude of the traces (crosses) as a function of $\gamma^2 g^2 \delta^2 D(\Delta - \delta/3)$. The solid line shows the expected decay for water with $D = 2.3 \times 10^{-9}$ m^2/s, which is in excellent agreement with the measurement.

3.6.2. Water Saturated Indiana Limestone

In Fig. 6, we show an example for a sample with a more complicated diffusion–relaxation distribution function. The sample is a core of Indiana limestone, saturated with water. This sedimentary rock has a porosity of 15% and a wide pore size distribution that spans at least three orders of magnitudes (*18*). This wide distribution of different environments for the spins is associated with different relaxation times and degrees of restriction for diffusion. It is interesting to study how the restricted diffusion and relaxation are correlated.

Within experimental uncertainty, the asymptotic echo shapes and transient effects were identical to those in the water

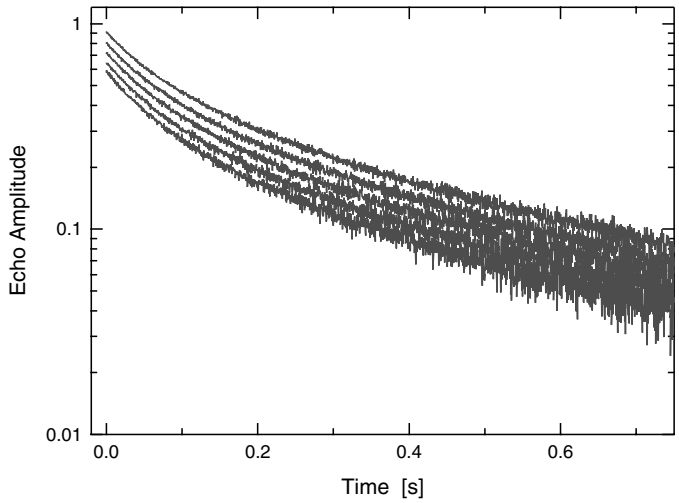

FIG. 6. Echo amplitudes for a sample of Indiana limestone saturated with water. The encoding time was $T_d = 20$ ms and the values of δ were chosen to lead to a diffusive attenuation of $\exp\{-0.2, -0.4 \ldots -1\}$ for unrestricted diffusion of water. At short times, the five traces are separated by a smaller amount, indicating restricted diffusion. The separation increases with time, which shows that spins with longer relaxation time are less restricted and that diffusion and relaxation are correlated.

measurements. The overall features of the data in Fig. 6 allow some general conclusions even before a detailed analysis is performed. Diffusion attenuates the five traces by a smaller amount than expected for free diffusion of water. This confirms that the diffusion of water is restricted. The data also show that the separation is increasing for the later echoes. This indicates that diffusion and relaxation are correlated: spins with long relaxation times are less restricted than spins with shorter relaxation times.

4. RESULTS

We have applied the new technique of measuring and extracting multidimensional distribution functions in grossly inhomogeneous fields to a number of different applications. We first present examples of measurements of diffusion–relaxation distribution functions for the characterization of fluids. We then show examples where the method is used to probe the geometry of porous media by extracting the correlations between restricted diffusion and relaxation. Finally, we also demonstrate the measurement of $T_1 - T_2$ correlation functions in strongly inhomogeneous fields.

4.1. Characterization of Fluids with $D - T_2$ Distribution Functions

As a first test, we applied the inversion algorithm discussed in Appendix B to the data on doped water shown in Fig. 5. The data consist of the amplitudes of the stimulated echo followed by 2000 echoes with an echo spacing of 375.2 μs for 24 different values of δ and $T_d = 30$ ms. Data compression reduces these 48 024 amplitudes to 23 significant data points. Optimization in this 23 dimensional subspace leads to the result of $f_{T_d}(D, T_{2\text{eff}})$ shown in Fig. 7. Here the regularization parameter is $\alpha = 10^{-2}$. Since for this sample $T_1 = T_2$, we do not have to distinguish between T_2 and $T_{2\text{eff}}$.

The results in Fig. 7 demonstrate that the algorithm can correctly extract the two-dimensional distribution function. The diffusion–relaxation distribution function and the projections along the D and T_2 dimensions shown on top and the right, respectively, both show the expected delta function like response.

A second example is shown in Fig. 8. The sample is the viscosity standard S3, a mixture of hydrocarbons with a kinematic viscosity of 4 mm^2/s at 25°C. It has a T_1 relaxation that is identical to its T_2 relaxation. In this case we acquired 4000 echoes for 24 different values of δ and $T_d = 30$ ms. The algorithm compressed the data to 25 significant amplitudes. The regularization parameter was 10^{-2}.

The two-dimensional distribution function $f_{T_d}(D, T_2)$ shows a strong linear correlation between diffusion coefficient and relaxation time. Both the one-dimensional distribution function of T_2 and diffusion coefficient are wider than in the case of water. It is interesting to compare this result with results by Lo *et al.* [19] and Straley [20] who have measured the mean diffusion coefficient and T_1 of a series of pure alkanes. They found that the points of these measurements lie on a line that is shown dashed in Fig. 8. This line coincides almost exactly with the ridge of the extracted $D - T_2$ distribution function of the mixture.

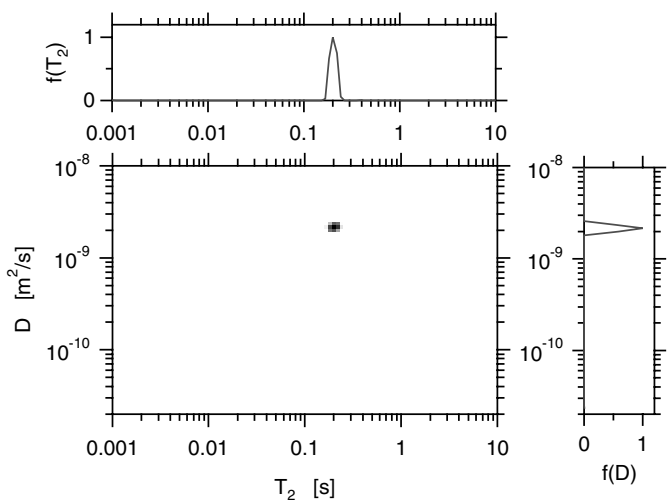

FIG. 7. Diffusion–relaxation distribution function extracted from measurements with the diffusion editing sequence on water doped with $NiCl_2$ in the presence of grossly inhomogeneous fields. The algorithm successfully extracts the delta-function like distribution function centered at the independently measured relaxation time of 202 ms and the diffusion coefficient of water, 2.3×10^{-9} m^2/s. On top and on the right, the projections along the diffusion and relaxation dimensions are shown, resulting in the one-dimensional T_2 and D distributions, respectively.

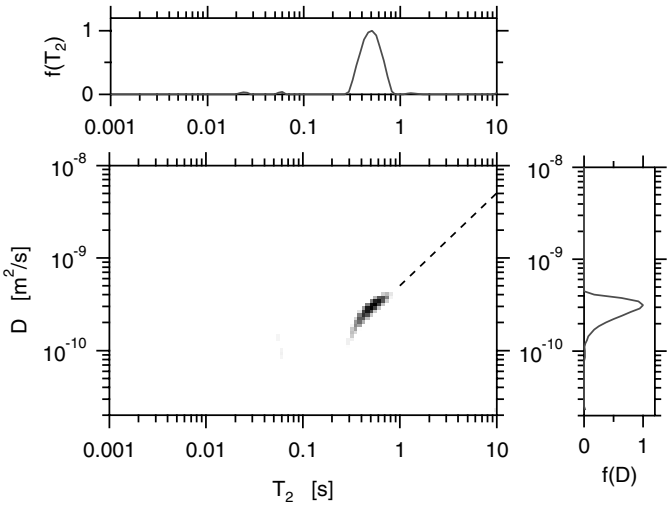

FIG. 8. Gray scale image of the diffusion–relaxation distribution function f_{T_d} for a sample of S3, a petroleum based viscosity standard, extracted from measurements in grossly inhomogeneous fields. The diffusion and T_2 distributions are both about half a decade wide with a strong linear correlation. The dashed line shows the correlation between mean diffusion coefficient and mean T_1 of pure alkanes reported in (*19, 20*).

4.2. Probing of Restricted Diffusion

In addition to using diffusion to identify and characterize fluids, diffusion can also be used to probe the geometry of porous media (*1–3*). Diffusion of fluid molecules filling the pore space of porous media is restricted by the presence of the pore walls. As a consequence, the time dependence of the mean squared displacement deviates from the Einstein relationship, $\langle x(t)^2\rangle = 2D_0t$, and the molecular diffusion coefficient D_0 has to be replaced by a time dependent diffusion coefficient, $D(t)$ (*21*). The value of $D(t)/D_0$ is a measure of the degree of restriction and its time dependence gives useful information about the geometry of the pore space. Here we demonstrate that it is possible to measure the correlation between the degree of restriction and relaxation.

An example of data for restricted diffusion measurements has been shown in Fig. 6. In these measurements, we have limited ourselves to small q values where the propagator can be well approximated by a Gaussian. We can then directly apply our inversion algorithm. With only five different diffusion encoding times, the extracted distributions are not well defined in the diffusion dimension. The quantity of interest is the first moment along the diffusion dimension,

$$\bar{D}(T_d, T_{2\text{eff}}) \equiv \frac{\int_0^\infty dD\, D f_{T_d}(D, T_{2\text{eff}})}{\int_0^\infty dD\, f_{T_d}(D, T_{2\text{eff}})}. \qquad [11]$$

The quantity $2\bar{D}(T_d,\ T_{2\text{eff}})T_d$ is the mean squared displacement during the diffusion time T_d along the gradient direction for spins with a relaxation time $T_{2\text{eff}}$.

We have performed three-dimensional experiments to measure the time dependent diffusion coefficient $\bar{D}(T_d,\ T_{2\text{eff}})$ for six different diffusion times and for relaxation times between 1 ms and a few seconds. For each diffusion time T_d, we acquired data for five different values of δ and 4000 echoes. We extracted a diffusion–relaxation distribution function for each value of T_d and then determined $\bar{D}(T_d, T_{2\text{eff}})/D_0$ by calculating the first moment over the diffusion dimension and normalize it with respect to D_0. The same regularization parameter was used for all six data sets. To assess the uncertainty in the extraction of $\bar{D}(T_d, T_{2\text{eff}})/D_0$ due to noise in the experimental data, we performed the following procedure: The data were first inverted using the algorithm as described. Using this solution, we calculated the fit to the amplitudes and added random Gaussian noise of the same amplitude as observed in the experiments. We then inverted this new synthetic data set and determined $\bar{D}(T_d, T_{2\text{eff}})/D_0$. This was repeated for 40 different noise realizations and the solutions were added. The resulting width along the diffusion dimension is therefore a measure of the uncertainty in extracting $\bar{D}(T_d, T_{2\text{eff}})/D_0$ from the data.

As an illustration, we show in Fig. 9, results for water in Indiana limestone. The gray scale was normalized to the maximum value for each diffusion time separately. The results show a clear correlation between the degree of restriction, $\bar{D}/D_0$, and relaxation time, $T_{2\text{eff}}$. With increasing diffusion time T_d,

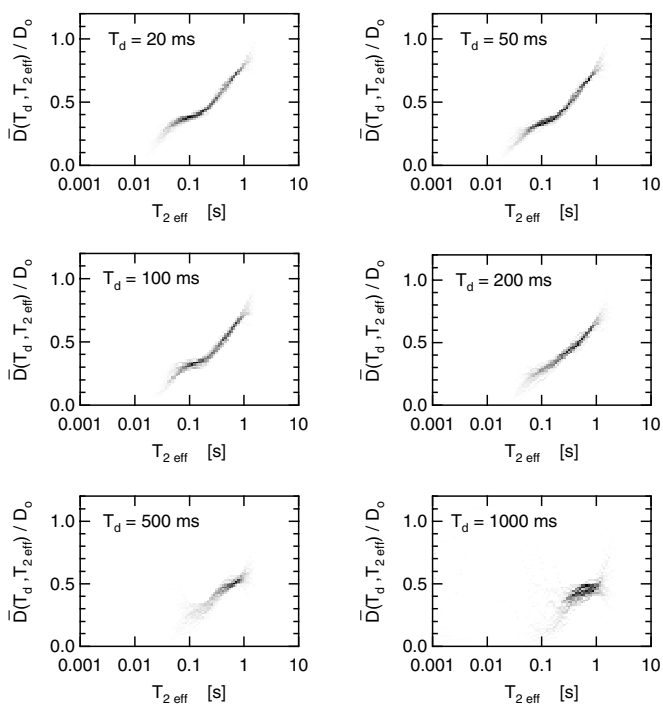

FIG. 9. Restricted diffusion versus relaxation time and diffusion time of water in Indiana limestone. For the six different diffusion times, T_d, indicated in the graphs the normalized mean squared displacement, $\bar{D}/D_0$, is plotted as a function of relaxation time, $T_{2\text{eff}}$. These results show a strong correlation between relaxation times and degree of restriction.

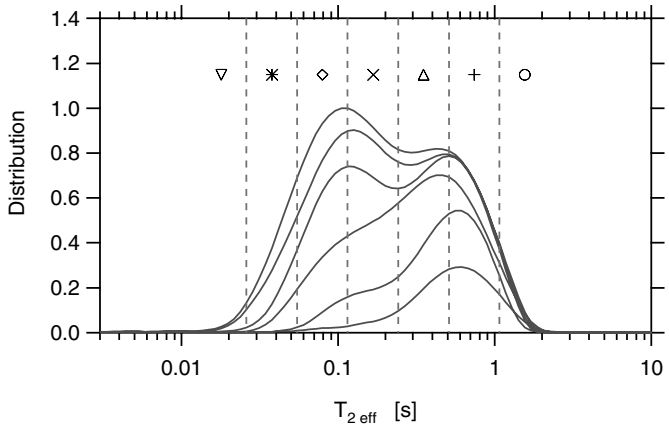

FIG. 10. Distributions of $T_{2\text{eff}}$ relaxation time for diffusion editing sequences for water in Indiana limestone, obtained by projecting the diffusion–relaxation distributions of Fig. 9 along the diffusion dimension. The six curves correspond to the different diffusion times of $T_d = 20$, 50, 100, 200, 500, and 1000 ms, respectively. The symbols on top identify the relevant relaxation time intervals for Fig. 11.

the magnetization of spins with short relaxation time decays during T_d and does not contribute to the results anymore. As shown by Eqs. [9] and [11], only the spins surviving at T_d contribute to $\bar{D}(T_d, T_{2\text{eff}})/D_0$. This is shown more clearly in Fig. 10, where the projections of Fig. 9 along the diffusion dimensions for the six different diffusion times are shown. According to Eq. [8], these projections correspond to $\iint dD\, dT_1\, f(D, T_{2\text{eff}}, T_1) \exp\{-T_d/T_1\}$ and can be used to obtain information about the relationship between T_1 and $T_{2\text{eff}}$. Assuming a constant $T_1/T_{2\text{eff}}$ ratio, we obtain $T_1/T_{2\text{eff}} = 1.8$. This is in full agreement with results shown in Section 4.4.

As the diffusion time is increased, diffusion becomes in general more restricted. The dependence of the normalized mean squared displacement, $\bar{D}(T_d, T_{2\text{eff}})/D_0$, on diffusion time, and resolved over relaxation times is shown in Fig. 11. For this display, the $T_{2\text{eff}}$ distributions were divided into 7 intervals as indicated in Fig. 10. For each relaxation time interval, we plot in Fig. 11 the average value of $\bar{D}/D_0$ for these spins from Fig. 9 versus the diffusion length $\sqrt{D_0 T_d}$. The intensities of each point are proportional to the number of surviving spins for the appropriate diffusion time and interval of relaxation times.

For each interval of relaxation times, the normalized mean squared displacement decreases with increasing diffusion time. Such information can be used to extract a local surface-to-volume ratio of the pore space occupied by spins with a given relaxation time and to calculate a surface relaxivity. A detailed analysis and comparison with other samples will be reported elsewhere. These data confirm that the quantity usually measured, the mean squared displacement of all surviving spins, can be misleading, as has been noted before (*22, 23*). At short diffusion times, signals from all relaxation times contribute to this averaged mean squared displacement, whereas at long times, only signals from long $T_{2\text{eff}}$ components contribute. This leads to a pronounced bias in the time dependence of the mean squared displacement of all surviving spins when restricted diffusion and relaxation are correlated. Even though the normalized mean squared displacement for each individual $T_{2\text{eff}}$ component decreases with increasing diffusion time in Fig. 11, the normalized mean squared displacement of all surviving spins is almost constant over the same range of diffusion times (*23*).

4.3. Effects of Susceptibility Induced Gradients

In Fig. 12, we show a representative example of results for restricted diffusion in sandstone. In this case, the relationship between the extracted diffusion coefficient and relaxation time is nonmonotonic. In contrast to carbonates where we find typically a monotonic dependence as shown in Fig. 9, the extracted diffusion coefficient for this sandstone is increasing as the relaxation times are decreased below 400 ms. Similar results are found for other sandstones. We interpret this as an effect due to the presence of internal gradients generated by the susceptibility contrast between the fluid and grains of the rock. With static gradients g used in the experiment, only the product

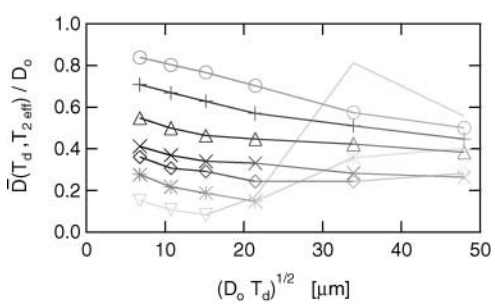

FIG. 11. Normalized mean squared displacement, $\bar{D}(T_d, T_{2\text{eff}})/D_0$, versus diffusion length, $\sqrt{D_0 T_d}$, for Indiana limestone. The different symbols indicate different intervals of relaxation times as indicated in Fig. 10. The intensities of the symbols are proportional to the number of surviving spins at the relevant diffusion time and interval of relaxation times.

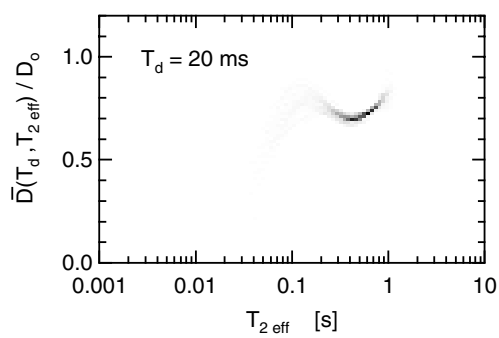

FIG. 12. Extracted values of $\bar{D}(T_d, T_{2\text{eff}})/D_0$ versus relaxation time $T_{2\text{eff}}$ for a sample of brine saturated Berea sandstone. The upturn at short relaxation time is caused by the presence of susceptibility induced gradients in the smaller pores. These gradients are at least comparable to the applied gradient of 13.2 G/cm, even though the applied field is only 414 G.

of $g^2\bar{D}(T_d,\ T_{2\text{eff}})$ can be measured. In the analysis leading to Fig. 12, we have assumed that the spins experience only the applied gradient of 13.2 G/cm. We have documented earlier that the susceptibility of sandstones is typically one to two orders of magnitude higher than in carbonates (*24*) and that the resulting internal gradients often exceed 13 G/cm in the smaller pores, even at such low fields as 414 G used in these experiments. The results in Fig. 12 confirm that the highest gradients are associated with the shorter relaxation times.

4.4. $T_1 - T_{2\text{eff}}$ Distributions

The technique of measuring diffusion–relaxation distribution functions in inhomogeneous fields can be adapted to measuring $T_1 - T_{2\text{eff}}$ distributions. We illustrate this here with an example using the pulse sequence shown in Fig. 1c. The modifications to the spin dynamics due to the large inhomogeneities have already been discussed in Ref. (*13*). In the experiment, we used 30 values of τ_1, spaced logarithmically between 1 ms and 10 s. In all cases, we acquired 4000 echoes with an echo spacing of 396 μs. Note that for the longest value of τ_1, the spins are fully relaxed at the time of the 90° pulse. Following (*13*), we first subtracted each data set from the fully relaxed data set: $\tilde{M}(\tau_1, t) = M(\tau_{1,\max}, t) - M(\tau_1, t)$. The echo shapes of $\tilde{M}(\tau_1, t)$ are then independent of τ_1 and quickly reach an asymptotic form with increasing echo number, analogous to the diffusion–relaxation case discussed above. We used this asymptotic echo shape as matched filter. The resulting amplitudes $A(\tau_1, kt_E)$ show a transient effect over the first few echoes, independent of τ_1, that are again completely analogous to the results shown in Fig. 4. After correcting for this transient effect, the amplitudes are related to the two-dimensional $T_1 - T_{2\text{eff}}$ distribution function by

$$A(\tau_1, kt_E) = \iint dT_1\, dT_{2\text{eff}}\, f(T_1, T_{2\text{eff}}) \exp\{-\tau_1/T_1\} \times \exp\{-kt_E/T_{2\text{eff}}\}. \quad [12]$$

The kernel is fully separable and the algorithm of (*17*) can be applied to invert the data and extract the two-dimensional distribution function.

The result of this procedure for a sample of Indiana limestone is shown in Fig. 13. This $T_1 - T_{2\text{eff}}$ distribution function extracted from measurements in strongly inhomogeneous fields is in excellent agreement with a previous determination based on measurements in a homogeneous field and reported in (*16*). In addition, note that the $T_{2\text{eff}}$ distribution obtained by projection from the $T_1 - T_{2\text{eff}}$ measurement and shown on top of Fig. 13 is in good agreement with the $T_{2\text{eff}}$ distribution obtained by projection from the earlier diffusion $-T_{2\text{eff}}$ measurement for the shortest diffusion encoding time, $T_d = 20$ ms, and shown as the top curve in Fig. 10.

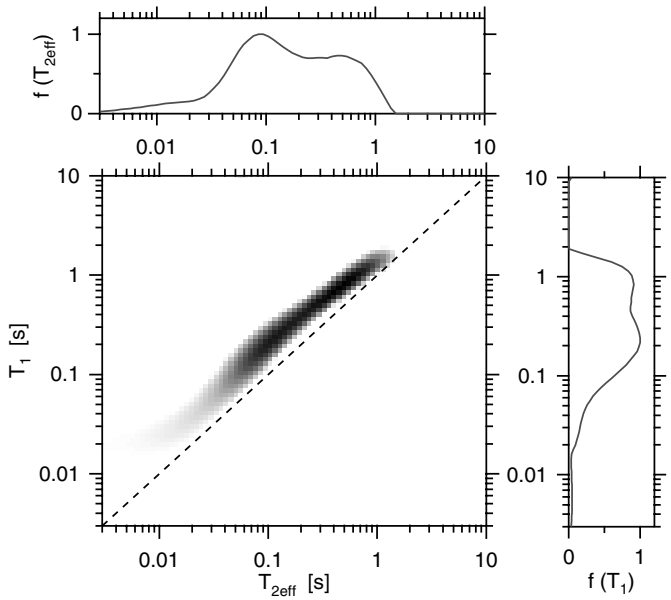

FIG. 13. $T_1 - T_{2\text{eff}}$ distribution for water in Indiana limestone measured in grossly inhomogeneous fields. The dashed line shows the line $T_1 = T_{2\text{eff}}$. The projections along the T_1 and $T_{2\text{eff}}$ dimensions result in the one-dimensional distributions shown on top and on the right, respectively. The two-dimensional distribution, extracted from measurements in strongly inhomogeneous fields, is in good agreement with the distribution reported in Ref. (*16*), measured on the same rock in a homogeneous field.

5. CONCLUSION

In this paper, we have introduced a new technique to measure quantitatively multidimensional distribution functions involving diffusion and relaxation, even in the presence of grossly inhomogeneous fields. This opens up new applications for the inside–out type of NMR measurements. We have demonstrated this with examples for fluid characterization and for the probing of the geometry of restrictions in porous media.

The technique developed is rather general and can be readily adopted to other applications or pulse sequences. We have presented the necessary tools to analyze the spin dynamics of modified sequences. For the editing part of the sequence, the magnetization is divided into different coherence pathways and the evolution can then be determined following (*13*). To calculate the evolution during the repeated refocusing cycles of the sequence, it is best to use the "method of effective rotation axis" developed in (*12, 15*).

The measurement of diffusion–relaxation distribution functions is a powerful means to characterize samples. We have demonstrated here the technique in the presence of grossly inhomogeneous fields. This information can also be obtained in more conventional ways using pulsed field gradients in a homogeneous field. In that case, the data inversion can be achieved with the same algorithm used here.

APPENDIX A: SPIN DYNAMICS IN INHOMOGENEOUS FIELDS

A.1. Editing Part of the Sequence

For the initial part of the sequence, the spin dynamics is treated exactly by considering the evolution along each coherence pathway separately. We illustrate this approach for the diffusion editing sequence shown in Fig. 1a that uses a stimulated echo as an editing element. The cases of inversion recovery and multiple echoes have already been treated in (*13*).

In this calculation, we follow the evolution of $M_{\pm 1} \equiv M_x \pm i M_y$, $M_0 \equiv M_z$. The magnetization following a number of pulses can be decomposed into contributions from different coherence pathways. Each coherence pathway can be characterized by a spectrum, a frequency independent diffusion attenuation, and a frequency independent relaxation attenuation (*13*). When more than one coherence contributes to the signal, the overall diffusion and relaxation attenuations are weighted sums of the individual contributions and become frequency dependent. To obtain kernels with a simple dependence on diffusion, it is therefore essential to ensure that only a single coherence pathway contributes to the signal. For the diffusion editing sequence with stimulated echo, this can be achieved with the 16 step phase cycling listed in Table 1.

The desired stimulated echo corresponds to the pathway $\{0 \to -1 \to 0 \to +1\}$. This pathway contributes only to the transverse magnetization, $m_{\mathcal{A}} = M_x + i M_y$, which is given by (*13*)

$$m_{\mathcal{A}} = \left\{\Lambda^{(3)}_{+1,0}\Lambda^{(2)}_{0,-1}\Lambda^{(1)}_{-1,0}\right\} \exp\left\{-q^2 D\left(\Delta - \frac{\delta}{3}\right)\right\} \times \exp\left\{-\frac{\Delta+\delta}{T_1} - 2\delta\left(\frac{1}{T_2} - \frac{1}{T_1}\right)\right\}. \quad [13]$$

Here we used the notation $q \equiv \gamma g \delta$. The $\Lambda^{(k)}_{l,j}$ are matrix transition elements of the kth pulse between initial coherence j and final coherence l. These matrix elements depend only on the pulse parameters of the kth pulse and the offset frequency, $\Delta\omega_0$, and are independent of diffusion and relaxation (*13*). For RF pulses of phase φ, duration t_p, frequency offset $\Delta\omega_0$, and RF field strength ω_1, the relevant elements are given by

$$\Lambda_{+1,0} = \frac{\omega_1}{\Omega}\left\{\frac{\Delta\omega_0}{\Omega}[1 - \cos(\Omega t_p)] - i\sin(\Omega t_p)\right\} e^{+i\varphi} \quad [14]$$

$$\Lambda_{-1,0} = \frac{\omega_1}{\Omega}\left\{\frac{\Delta\omega_0}{\Omega}[1 - \cos(\Omega t_p)] + i\sin(\Omega t_p)\right\} e^{-i\varphi} \quad [15]$$

$$\Lambda_{0,-1} = \frac{1}{2}\frac{\omega_1}{\Omega}\left\{\frac{\Delta\omega_0}{\Omega}[1 - \cos(\Omega t_p)] + i\sin(\Omega t_p)\right\} e^{+i\varphi} \quad [16]$$

Here $\Omega \equiv \sqrt{\Delta\omega_0^2 + \omega_1^2}$ is the nutation frequency.

The selection of the desired coherence pathway through phase cycling is based on the dependence of the matrix elements $\Lambda^{(k)}_{l,j}$ on the phase of the RF pulses, ϕ_k, that goes like $e^{i(l-j)\phi_k}$ (*13*). Therefore, the phase of the stimulated echo, ϕ_{ste}, depends on the phases of the first three RF pulses, ϕ_i, as $\Delta\phi_{ste} = -\Delta\phi_1 + \Delta\phi_2 + \Delta\phi_3$, valid for an arbitrary offset frequency. The phases of the RF pulses and acquisition in Table 1 are varied systematically according to this relationship such that the contributions of the stimulated echo add coherently whereas the contributions from all other possible coherence pathways are eliminated. Standard phase cycling of the 180° pulses of the CPMG part is also included to eliminate pulse ringing and dc offsets.

To compensate for finite pulse width effects, the spacing of the initial two 90° pulses is reduced by $2t_{90}/\pi$ from δ. As discussed in (*13*), this adds a phase factor $e^{+i2\Delta\omega_0 t_{90}/\pi}$ to Eq. [13] that compensates the frequency dependent phase of $\Lambda^{(3)}_{+1,0}\Lambda^{(2)}_{0,-1}\Lambda^{(1)}_{-1,0}$ to first order.

A.2. CPMG Part of the Sequence

The spin dynamics describing the repeated refocusing by the long string of 180° pulses has to be analyzed differently from the initial editing part of the sequence. Off resonance, a very large number of different coherence pathways contribute to the signal of the later echoes, preventing the direct application of the coherence pathway approach. We use instead the "method of effective rotation axis" (*12*). It is based on the analysis of the propagator over a single refocusing cycle, which is to first order a rotation.

The diffusion editing sequence can be viewed as a modified CPMG sequence where the initial 90° pulse is replaced by the stimulated echo sequence that acts as an effective 90° pulse with diffusion sensitivity. For simplicity, we assume here that the echo spacing t_E is short enough to make additional diffusion effects insignificant during the repeated refocusing parts of the sequence. Note that for measurements on rocks, this requires low magnetic fields of the order of 2 MHz or lower, otherwise diffusion in field inhomogeneities induced by susceptibility contrasts in the sample becomes important (*24*).

For echo spacings t_E much shorter than the relaxation time, the evolution from one echo to the next is well described by an overall rotation around an axis $\hat{n}$ with an angle α. Both $\hat{n}$ and α depend on the offset frequency, $\Delta\omega_0$, and the RF field strength, ω_1. With this notation and ignoring relaxation for the moment, a simple expression is obtained for the magnetization $\vec{m}(kt_E)$ after k refocusing cycles:

$$\vec{m}(kt_E) = \hat{n}(\hat{n}\cdot\vec{m}_{\mathcal{A}}) + [\hat{n}\times\vec{m}_{\mathcal{A}}]\sin(k\alpha) + [\vec{m}_{\mathcal{A}} - \hat{n}(\hat{n}\cdot\vec{m}_{\mathcal{A}})]\cos(k\alpha). \quad [17]$$

Here $\vec{m}_{\mathcal{A}}$ is the magnetization at the end of the editing part of the overall sequence, i.e., at a time $t_E/2$ before the first 180° refocusing pulse, and is given by Eq. [13].

The components $n_y \equiv \hat{n} \cdot \hat{y}$ and $n_z \equiv \hat{n} \cdot \hat{z}$ are given by

$$n_y = \frac{\omega_1}{\Omega} \frac{\sin\beta_2}{\left\{\left[\frac{\omega_1}{\Omega}\sin\beta_2\right]^2 + \left[\sin\beta_1\cos\beta_2 + \frac{\Delta\omega_0}{\Omega}\cos\beta_1\sin\beta_2\right]^2\right\}^{1/2}} \quad [18]$$

$$n_z = \frac{\sin\beta_1\cos\beta_2 + \frac{\Delta\omega_0}{\Omega}\cos\beta_1\sin\beta_2}{\left\{\left[\frac{\omega_1}{\Omega}\sin\beta_2\right]^2 + \left[\sin\beta_1\cos\beta_2 + \frac{\Delta\omega_0}{\Omega}\cos\beta_1\sin\beta_2\right]^2\right\}^{1/2}}, \quad [19]$$

where

$$\beta_1 = \Delta\omega_0 t_E/2 \quad [20]$$

$$\beta_2 = \Omega\, t_{180}/2. \quad [21]$$

The component of $\hat{n}$ along $\hat{x}$ is always zero. The angle of rotation, α, is given by

$$\cos\left(\frac{\alpha}{2}\right) = \cos\beta_1\cos\beta_2 - \frac{\Delta\omega_0}{\Omega}\sin\beta_1\sin\beta_2. \quad [22]$$

Here we have assumed that $0 \le \alpha < 2\pi$.

In sufficiently inhomogeneous fields, the distribution of angles α is wide enough so that the second and third terms in Eq. [17] average out after only a few echoes and do not contribute to the measured echo amplitudes anymore. The echo shape becomes then independent of the echo number, k. For extended samples in a strayfield setup, we have shown that these extra two terms are only noticeable for the first and second echoes of a CPMG sequence (*12, 15*). For the later echoes, it is therefore sufficient to consider only the first term in Eq. [17].

A.2.1. Relaxation

Relaxation leads to an attenuation of this first term with a decay rate $1/T_{2\text{eff}}$ that is a weighted sum of the longitudinal and transverse relaxation rate (*12*),

$$\frac{1}{T_{2\text{eff}}} = \frac{1}{T_2} - (\hat{n}\cdot\hat{z})^2\left(\frac{1}{T_2} - \frac{1}{T_1}\right). \quad [23]$$

Here we have assumed that the echo spacing t_E is much shorter than the relaxation time T_2, or more precisely $t_E \ll \frac{\alpha}{2\pi}T_2$. Exactly on resonance, $\hat{n}\cdot\hat{z} = 0$ and the measured relaxation time $T_{2\text{eff}} = T_2$. However, off resonance, the measured relaxation time is in general a combination of T_2 and T_1. For samples in very inhomogeneous fields, the average value of $\langle(\hat{n}\cdot\hat{z})^2\rangle$ is typically of the order of 10% (*12*). Strictly speaking, we measure therefore not $D - T_2$ correlations, but $D - T_{2\text{eff}}$ correlations. Using the sequence shown in Fig. 1c, it is possible to measure $T_1 - T_{2\text{eff}}$ correlations in the same experimental arrangement and use them to transform $D - T_{2\text{eff}}$ correlations to $D - T_2$ correlations. For our applications, the difference between T_2 and $T_{2\text{eff}}$ is typically no more than a few percent.

APPENDIX B: ALGORITHM FOR DATA INVERSION

Given the measured echo amplitudes, $A(t, \delta)$, the goal is to extract the diffusion–relaxation distribution function that best describes this data according to Eq. [10]. For this purpose, it is convenient to rewrite Eq. [10] for the discrete times of the experiments in matrix form:

$$A = K_1 F K_2' + E. \quad [24]$$

Here A is the matrix of measured echo amplitudes, K_1 is the matrix of the diffusion kernel, $\exp\{-\gamma^2 g^2 \delta^2 D(\Delta - \frac{\delta}{3})\}$, K_2 is the matrix of the relaxation kernel, $\exp\{-t/T_{2\text{eff}}\}$, and F is the matrix of the diffusion–relaxation distribution function, $f_{T_d}(D, T_{2\text{eff}})$. E indicates the noise term, assumed to be Gaussian with zero mean.

It is well known that the inversion of Eq. [24] with such smooth kernels is ill-conditioned, i.e., small changes in the noise term lead to vastly different inversion results. In addition, the data matrix is in general very large. For a typical case of 5 diffusion encodings and a few thousand echoes, the data matrix has about 10^4 elements. These two complications make an inversion based on a simple least squared optimization of Eq. [24] both unstable and very slow. In addition, the solution for the distribution function is not guaranteed to be positive.

We have recently developed an efficient algorithm to solve two-dimensional problems of the form of Eq. [24] with non-negativity constraint in an optimization framework (*17*). This algorithm has already been applied by Song *et al.* (*16*) to obtain $T_1 - T_2$ distribution functions of water saturated rocks measured in a homogeneous field at 2 MHz. We have adapted the algorithm for our problem of diffusion–relaxation inversion.

The algorithm consists of three main steps. In the first step, the highly redundant data are compressed. This is achieved by performing separate singular value decompositions of each kernel, K_1 and K_2. This results in the singular values $s_1^{(j)}$ and $s_2^{(k)}$ for the two kernels, respectively. The data are then projected into the subspace associated with the most significant singular values. In our application, we choose this subspace by requiring that the product of the associated singular values $s_1^{(j)} s_2^{(k)}$ be larger than 10^{-3} times the largest such product. We find that the exact condition defining this subspace is not critical. The subspace has to be large enough to include all significant features, but small enough to avoid large noise amplification. In our applications, this compression leads to a large data reduction from over 10^4 points to typically between 17 and 25 data points.

The second step consists of an optimization within this reduced data space. To assure stability, we include a regularization term of the form $\alpha\|F\|^2$:

$$\hat{F} = \arg\min_{F\ge 0} \|\tilde{A} - \tilde{K}_1 F \tilde{K}_2\|^2 + \alpha\|F\|^2. \quad [25]$$

The tilde indicates that the data were compressed and that the kernels operate only in this subspace. The nonnegativity constraint complicates this optimization. In our routine (*17*), we take advantage of the algorithm by Butler, Reeds, and Dawson (BRD) (*25*) to map this constrained problem onto an unconstrained optimization problem. This unconstrained problem can then be solved in a straightforward manner.

In the third step, the regularization parameter α is determined self-consistently. Large values of α lead to broad, featureless distribution functions that do not fit the data very well. As α is reduced, the fitting error gets initially reduced, but ultimately the solution becomes unstable and spurious features appear in F. Roughly speaking, the optimal regularization parameter α_{opt} is chosen such that it results in the smoothest distribution function that still fits the data. Reducing α below α_{opt} barely reduces the fitting error, but leads to instabilities. Increasing α leads to noticeably larger fitting errors. As discussed in (*17*), there are several methods to determine α_{opt}. In our application, we have used mainly the method first proposed in the BRD algorithm (*25*).

ACKNOWLEDGMENTS

We thank Y. Q. Song for discussions on the data inversion, C. Straley for sharing his insight into diffusion and relaxation properties of hydrocarbon fluids, U. Scheven for discussion on experimental issues, and D. Freed and P. Sen for discussions on theoretical issues.

REFERENCES

1. D. G. Cory and A. N. Garroway, Measurement of translational displacement probabilities by NMR: An indicator of compartmentation, *Magn. Reson. Med.* **14,** 435–444 (1990).

2. P. T. Callaghan, A. Coy, D. MacGowan, K. J. Packer, and F. O. Zelaya, Diffraction-like effects in NMR diffusion studies of fluids in porous solids, *Nature* **351,** 467–469 (1991).

3. P. P. Mitra, P. N. Sen, L. M. Schwartz, and P. Le Doussal, Diffusion propagator as a probe of the structure of porous media, *Phys. Rev. Lett.* **68,** 3555–3558 (1992).

4. K. R. Brownstein and C. E. Tarr, Importance of classical diffusion in NMR studies of water in biological cells, *Phys. Rev. A* **19,** 2446 (1979).

5. W. E. Kenyon, P. I. Day, C. Straley, and J. F. Willemsen, A three-part study of NMR longitudinal relaxation properties of water-saturated sandstones, *Soc. Petrol. Eng. Form. Eval.* **3,** 622–636 (1988); Erratum, *Soc. Petrol. Eng. Form. Eval.* **4,** 8 (1989).

6. F. D'Orazio, J. C. Tarczon, W. P. Halperin, K. Eguchi, and T. Mizusaki, Application of nuclear magnetic resonance pore structure analysis to porous silica glass, *J. Appl. Phys.* **65,** 742–751 (1989).

7. R. L. Kleinberg, "Encyclopedia of Nuclear Magnetic Resonance," Vol. 8, Chap. Well logging, pp. 4960–4969, Wiley, Chichester (1996).

8. G. Eidmann, R. Savelsberg, P. Blümler, and B. Blümich, The NMR MOUSE, a mobile universal surface explorer, *J. Magn. Reson. A* **122,** 104–109 (1996).

9. R. Kimmich and E. Fischer, One- and two-dimensional pulse sequences for diffusion experiments in the fringe field of superconducting magnets, *J. Magn. Reson. A* **106,** 229–235 (1994).

10. P. J. McDonald, Stray field magnetic resonance imaging, *Prog. Nucl. Magn. Reson. Spectrosc.* **30,** 69–99 (1997).

11. C. A. Meriles, D. Sakellariou, H. Heise, A. J. Moulé, and A. Pines, Approach to high-resolution ex situ NMR spectroscopy, *Science* **293,** 82–85 (2001).

12. M. D. Hürlimann and D. D. Griffin, Spin dynamics of Carr–Purcell–Meiboom–Gill-like sequences in grossly inhomogeneous B_0 and B_1 fields and application to NMR well logging, *J. Magn. Reson.* **143,** 120–135 (2000).

13. M. D. Hürlimann, Diffusion and relaxation effects in general stray field NMR experiments, *J. Magn. Reson.* **148,** 367–378 (2001).

14. S. Peled, D. G. Cory, S. A. Raymond, D. A. Kirschner, and F. A. Jolensz, Water diffusion, T_2, and compartmentation in frog sciatic nerve, *Magn. Reson. Med.* **42,** 911–918 (1999).

15. M. D. Hürlimann, Carr–Purcell sequences with composite pulses, *J. Magn. Reson.* **152,** 109–123 (2001).

16. Y.-Q. Song, L. Venkatarmanan, M. D. Hürlimann, M. Flaum, P. Frulla, and C. Straley, $T_1 - T_2$ correlation spectra obtained using a fast two-dimensional Laplace inversion, *J. Magn. Reson.* **154,** 261–268 (2002).

17. L. Venkataramanan, Y.-Q. Song, and M. D. Hürlimann, Solving Fredholm integrals of the first kind with tensor product structure in 2 and 2.5 dimensions, *IEEE Trans. Signal Process.* **50,** 1017–1026 (2002).

18. R. W. Mair, G. P. Wong, D. Hoffmann, M. D. Hürlimann, S. Patz, L. M. Schwartz, and R. L. Walsworth, Probing porous media with gas diffusion NMR, *Phys. Rev. Lett.* **83,** 3324–3327 (1999).

19. S. Lo, G. J. Hirasaki, W. V. House, and R. Kobayashi, Correlations of NMR relaxation time with viscosity, diffusivity, and gas/oil ratio of methane/hydrocarbon mixtures, *in* "Proceedings of the 2000 Annual Technical Conference and Exhibition of the Society of Petroleum Engineers, SPE 63217," pp. 757–771 (2000).

20. C. Straley, private communication, 2001.

21. D. E. Woessner, NMR spin-echo self-diffusion measurements on fluids undergoing restricted diffusion, *J. Phys. Chem.* **67,** 1365–1367 (1963).

22. P. N. Sen, L. M. Schwartz, P. P. Mitra, and B. I. Halperin, Surface relaxation and the long-time diffusion coefficient in porous media: Periodic geometries, *Phys. Rev. B* **49,** 215–225 (1994).

23. M. D. Hürlimann, K. G. Helmer, L. L. Latour, and C. H. Sotak, Restricted diffusion in sedimentary rocks: Determination of surface-area to volume ratio and surface relaxivity, *J. Magn. Reson. A* **111,** 169–178 (1994).

24. M. D. Hürlimann, Effective gradients in porous media due to susceptibility differences, *J. Magn. Reson.* **131,** 232–240 (1998).

25. J. P. Butler, J. A. Reeds, and S. V. Dawson, Estimating solutions of first kind integral equations with nonnegative constraints and optimal smoothing, *SIAM J. Numer. Anal.* **18,** 381–397 (1981).